Microcirculation

Fractal Characterization of Retinal Microvascular Network Morphology During Diabetic Retinopathy Progression

Journal:	*Microcirculation*
Manuscript ID	UMIC-2018-0129.R1
Manuscript Type:	Original Research
Date Submitted by the Author:	n/a
Complete List of Authors:	Popovic, Natasa; University of Montenegro, Faculty of Medicine, Medical Physiology Lipovac, Mirko; University of Montenegro, Faculty of Medicine, Medical Physiology Radunovic, Miroslav; University of Montenegro, Faculty of Medicine Ugarte, Jurgi; ULMA Embedded Solutions Isusquiza, Erik; ULMA Embedded Solutions Beristain, Andoni; VICOMtech Moreno, Ramón; VICOMtech Aranjuelo, Nerea; VICOMtech Popovic, Tomo; University of Donja Gorica, Faculty for Information Systems and Technologies
Keywords:	diabetic retinopathy, fractal analysis, multifractals, lacunarity, microvascular network morphology

Fractal Characterization of Retinal Microvascular Network Morphology During Diabetic Retinopathy Progression

Authors: Natasa Popovic[a], Mirko Lipovac[a], Miroslav Radunovic[a], Jurgi Ugarte[b], Erik Isusquiza[b], Andoni Beristain[c], Ramón Moreno[c], Nerea Aranjuelo[c], and Tomo Popovic[d]

Running title: Microvascular geometry in diabetes

[a]Faculty of Medicine, University of Montenegro, Krusevac bb, 81000 Podgorica, Montenegro

[b]ULMA Embedded Solutions, Garagaltza auzoa 51, 20560 Oñati, Gipuzkoa, Spain

[c]Vicomtech, Mikeletegi Pasealekua 57, 20009 San Sebastián, Gipuzkoa, Spain

[d]Faculty for Information Systems and Technologies, University of Donja Gorica, Oktoih 1, 81000 Podgorica, Montenegro

Sources of support: The research is funded in part by the RETINAL project, EU Framework Programme for Research and Innovation - SME instrument, Horizon 2020 Grant Agreement No. 806245.

Corresponding author: Natasa Popovic, npopovic@ucg.ac.me, Faculty of Medicine, University of Montenegro, Krusevac bb, 81000 Podgorica, Montenegro

ABSTRACT

Objective: The study aimed to characterize morphological changes of the retinal microvascular network during the progression of diabetic retinopathy.

Methods: Publicly available retinal images captured by a digital fundus camera from DIARETDB1 and STARE databases were used. The retinal microvessels were segmented using the automatic method and vascular network morphology was analyzed by fractal parametrization such as box-counting dimension, lacunarity, and multifractals.

Results: The results of the analysis were affected by the ability of the segmentation method to include smaller vessels with more branching generations. In cases where the segmentation was more detailed and included a higher number of vessel branching generations, increased severity of diabetic retinopathy was associated with increased complexity of microvascular network as measured by box-counting and multifractal dimensions, and decreased gappiness of retinal microvascular network as measured by lacunarity parameter. This association was not observed if the segmentation method included only 3-4 vessel branching generations.

Conclusions: Severe stages of diabetic retinopathy could be detected non-invasively by using high resolution fundus photography and automatic microvascular segmentation to the high number of branching generations, followed by fractal analysis parametrization. This approach could improve risk stratification for the development of microvascular complications, cardiovascular disease and dementia in diabetes.

KEY WORDS:

diabetic retinopathy, fractal analysis, multifractals, lacunarity, microvascular network morphology

LIST OF ABBREVIATIONS AND SYMBOLS:

DR – diabetic retinopathy

OCTA – optical coherence tomography - angiography

DM1 – type 1 diabetes mellitus

DM2 – type 2 diabetes mellitus

PDR – proliferative diabetic retinopathy

Db – box-counting fractal dimension

Λ – mean lacunarity

STARE – Structured Analysis of Retina

SD – standard deviation

DIARETDB1 – Standard Diabetic Retinopathy Database Calibration level 1

ANOVA – analysis of variance

ROI – region of interest

INTRODUCTION

According to the World Health Organization global report on diabetes mellitus (DM) from 2016, an estimated number of adults living with DM increased from 108 million in 1980 to 422 million 2014, and the global age-standardized prevalence of DM increased from 4.7% to 8.5% in the same period (1). In accordance with this, the prevalence of DM has been increasing over time in the United States, especially in the adults older than 65 (2). In most of the world life expectancy has doubled in the past century (3), so the burden of diabetes is expected to rise significantly as the number of individuals with DM increases. Since the treatment of DM complications can cause 11-fold increase in direct medical cost of type 2 diabetes (4), early diagnosis and timely treatment of DM complications is extremely important. Diabetic retinopathy (DR) is a microvascular complication of diabetes and one of the leading causes of loss of vision in middle income and industrialized countries in the world (5). Therefore, the American Diabetic Association currently recommends referral of individuals with type 1 diabetes (DM1) to their first ophthalmologic exam 5 years after the initial diagnosis of diabetes, and with type 2 diabetes (DM2) at the time of initial diagnosis (6). This recommendation is based on the fact that at the time of the first diagnosis of diabetes, more than 30% of patients already have microvascular complications, but more than 40% of them have no associated symptoms (7, 8).

Fundoscopic examination and visualization of retinal vascular network can give us not only the information related to the presence and severity of diabetic retinopathy, but also on the condition of the microvascular network in the entire organism, and potential presence of other microvascular complications of DM (9). Numerous studies have confirmed that microvascular disease represents an independent risk factor for development of cardiovascular complications in DM1 and DM2 (9-11). Moreover, Exalto et al. have shown that individuals with severe diabetic retinopathy have significantly increased risk for the development of dementia (12). Taken together, these reports show that the assessment of the retinal microvasculature in patients with diabetes can be important not only for the prevention and treatment of blindness, but also for the timely prevention and treatment of other

microvascular complications of DM, as well as cardiovascular complications and possibly dementia. Therefore, there is a need for the development of a simple, non-invasive method for DR screening and DR severity staging in a large population in the primary care setting. Inclusion of family physicians in this process of DR screening focused on early detection of DR and prevention of blindness has already been shown to be very effective (13). One of the methods that could be used as a screening tool is analysis of 2-dimensional color images of retina captured by digital fundus cameras. These cameras are affordable, becoming smaller in size and portable, and are able to capture high resolution retinal images of exceptional quality (14, 15).

The complexity of the microvascular network is affected by DR. The studies using fractal analysis to explore this phenomenon report conflicting results: while some researchers report increased, the others report decreased microvascular complexity in DR (16-18). Morphological features typically found in DR such as arteriolar pruning and neovascularization (19) can affect complexity of microvascular network morphology in the opposing ways. While arteriolar pruning could decrease complexity, neovascularization that is present only in the advanced stages of DR could increase complexity of the microvascular network. Therefore, the observed inconsistencies in these reports may be related to different stages of DR being studied. Different resolution of details in the images of vascular network used in these studies could be the cause of these disagreements as well.

The goal of the study presented here was to characterize the changes of the retinal microvascular network morphology in various stages of the progression of DR, in retinal fundus images with a high level of details showing a high number of vessel branching generations, as well as in retinal images with a low level of details showing a lower number of vessel branching generations. We aimed to accomplish this in three steps (Figure 1). First, 2-dimensional color retinal images of patients with DM were segmented by using an automatic method for blood vessel segmentation. Next, we used the fine and the coarse filtering settings and thresholding on each image, to generate one image with a low number of vessel branching generations, and the second corresponding image that is very detailed and shows a high number of vessel branching generations. Finally, we compared vascular network

morphology in various stages of DR progression by fractal analysis parameterization in both groups of images. We hypothesized that 1) this approach would detect changes in the microvascular network morphology typical for different stages of DR, and 2) that DR affects microvascular network complexity globally, but the observed changes are different depending on whether the smaller vessel branches from higher branching generations are included in the analysis.

We show that the results of fractal analysis are indeed affected by the number of vessel branching generations included in the analysis. More importantly, the study describes a simple approach that could be used to detect severe stages of DR even in primary care settings. This could improve the stratification of patients with DR according to the risk for development of other diabetic microvascular complications and allow for their timely referral to appropriate specialists, improvement of treatment outcomes, as well as the reduction of medical costs.

MATERIALS AND METHODS

1) Retinal images and diabetic retinopathy staging

Raw retinal images from publicly available Standard Diabetic Retinopathy Database Calibration level 1 (DIARETDB1) were used in the study (14, 15). This database consists of 89 color images of retina, with 1500X1152 pixel resolution, most of which contain changes consistent with DR. All the raw fundoscopic images in DIARETDB1 database were captured by using the same digital fundoscopic camera at 50-degree field of view under conditions commonly encountered in real life. All images were centered on the macula of either the left or right eye. Other imaging settings of the camera were variable and automatically controlled by the system and were not recorded. For the purpose of automatic segmentation, most of the raw images from DIARETDB1 database were underexposed and therefore too dark. Since the flash intensity settings were variable, and the illumination settings were not recorded at the time the images were captured, we estimated them by using the GIMP image editor's Value histogram function, which calculates basic brightness information (20). Illumination (i.e. exposure) was estimated by the mean value of the histogram (Figure 2A), while the tonal range was

estimated by standard deviation of the histogram (data not shown). The mean estimated light exposure values of the images from DIARETDB1 ranged from 44.8 to 188.8. The twenty images that were sufficiently illuminated belong to the 4th quartile on the graph showing distribution of images by estimated light exposure (Figure 2B), and they were used in further analysis.

Since the severity of DR in each image was not specified, three of our medical experts independently determined the stage of DR for each image in the DIARETDB1 database by following the Early Treatment Diabetic Retinopathy Study Research Group recommendations (21). The group of medical experts consisted of one ophthalmologist and two medical doctors – general practitioners. In order to make sure they used consistent grading criteria, all experts were required to complete the on-line self-directed diabetic retinopathy grading course and successfully pass the competency-based exam (22). The retinal images were initially staged into 5 groups: normal looking with no signs of DR (stage 0), mild (stage 1), moderate (stage 2), severe non-proliferative (stage 3), and proliferative DR (stage 4). In cases where there were slight differences in staging among the medical experts, the stage was determined based on the majority opinion. Since our study focused on a subset of only 20 samples that were adequately illuminated, the images were finally grouped into 3 groups according to severity of DR (Table 1): normal looking (5 images with no signs of DR-stage 0), moderate DR (6 images with signs of moderate DR-stage 2), and severe DR (5 images with severe non-proliferative DR-stage 3, and 4 images with signs of severe proliferative DR-stage 4). In this group of 20 images, there were no images corresponding mild DR-stage 1. The overall agreement among the graders was 80%, with a good value for free-marginal kappa of 0.70 (95%CI = 0.49 - 0.91). This inter-rater variability in our study was comparable to other studies using the same method of measurement of inter-rater variability (23, 24). Among the 3 groups of images, there was no significant difference in the estimated light exposure, and in the estimated tonal range (data not shown).

In addition, the raw retinal images, from the publicly available Structured Analysis of Retina (STARE) database were used in the study (25, 26). The STARE database contains 402 annotated color images captured at 35-degree field of view with 700X605 pixel resolution. Out of these we used a subset of

images that were either normal looking or associated with the diagnosis of proliferative diabetic retinopathy (PDR), and that were of adequate quality as previously described (27). In this subset ten images did not have any pathological changes, while 9 were associated with the diagnosis of PDR. Some of the images were centered on the macula, but some were centered on the optic disc. All 19 images belonging to the STARE database were adequately illuminated and the mean estimated exposure values ranged from 101.7 to 176.9. The cumulative list of samples used in the study is shown in Table 1. For both databases, the additional patient information related to demographic data, history of present illness, previous medical history, type of medication therapy, compliance with the therapy, as well as the level of hemoglobin A1c and other relevant laboratory values, were not available. The data associated with either set of images also did not specify the type of DM, and if the normal looking images come from healthy individuals or from those diagnosed with diabetes that did not develop signs of DR.

2) Automatic segmentation of the raw images

The raw images were segmented by using the software program developed as a part of the non-invasive medical imaging project focused on the diagnosis and early detection of non-communicable diseases (28). An enhanced version of the Convolutional Neural Network (CNN) based on the Deep Retinal Image Understanding network (29) was used to develop the software for the retinal microvasculature detection. The network was trained and validated with images of different databases containing retinal fundus images with their corresponding ground truth images of microvascular networks: STARE, DRIVE, CHASE_DB1 and HRF (26, 30-32). Horizontal and vertical flip based data augmentation was used (28). Stochastic gradient descent was used as minimization method, for 13560 iterations, with an initial learning rate of 0.001, which was reduced to 0.0001 after half of the training iterations were completed. Softmax cost function was employed, in order to obtain a pixel wise error measurement. This cost function was normalized given the unbalanced scenario between background and vessel pixel number, using that ratio as normalization value.

The automatic segmentation of both sets of images was performed by an expert who was blinded to

the diagnosis associated with each image and to the results of DR staging. The automatic segmentation resulted in a set of gray scale images, representing the vesselness probability for each pixel in a 0-255 range.

3) Selection of the region of interest

Diabetic retinopathy has a progressive course, and pathological changes close to macula, the area central vision, represent the most serious threat to eyesight (5). Recent advances in optical coherence tomography – angiography (OCTA) allow visualization of the detailed 3-dimensional anatomy of vascular plexuses in healthy retina. OCTA showed that in the healthy retina the most dramatic changes in vessel density are present around foveolar avascular zone (33). For these reasons our research is primarily focused on the region of interest (ROI) microvascular network morphology in a circular area of retina that includes macula in the center and the optic disc at the periphery of each image. For the DIARETDB1 database ROI was a circular area measuring 1000 pixels in diameter, containing the macula in the center and the complete optic disc. Since the images from the STARE database had a lower resolution and were centered inconsistently, the ROI was defined as a circular area of 500 pixels in diameter, centered either on the macula or on the optic disc. Each ROI was cropped using the GIMP image processor.

4) Image binarization and filtering

Binarization was performed by using ImageJ software and its Mexican hat wavelet filter followed by adjusting the image threshold to maximum (white pixel) (34). The Mexican hat filter is commonly used for feature detection by applying Laplacian of Gaussian filter to a two-dimensional image. In this process we used the radius of 5 pixels as a fine filter, and the radius of 2 pixels as a coarse filter to get two sets of binarized images for each database. The application of the coarse filter yielded images with low number, while the fine filter yielded images of with high number of vessel branching generations (Figure 3).

5) Box-counting, lacunarity, and multifractal analysis of the segmented images

Box-counting, lacunarity analysis, and multifractal analysis of both sets of the binarized images were

done by using FracLac feature of the ImageJ software (34) with the default settings as described in Popovic at al. and Karperien et al (27, 35). In short, in box-counting analysis the image is broken into smaller square boxes of a specific predetermined size by the fractal analysis software. Each box that contains the foreground blood vessel pixels is assigned a value of 1, while all other boxes hold the value of 0. Following that, the software counts the number of boxes containing foreground pixels and calculates the fractal dimension, also called the box-counting dimension (Db). The higher the fractal dimension, the higher the complexity and self-similarity of the image. The mean lacunarity (Λ) represents inhomogeneity or gappiness caused by the gaps in the binarized image.

Box-counting dimension calculation is a type of monofractal analysis. The concept applied in multifractal analysis is analogous to applying filters to an image to emphasize certain features that otherwise are not obvious (35). Structures that have monofractal nature are not affected by this process. While box-counting counts the number of boxes that contain foreground pixels, multifractal analysis counts the number of foreground pixels for each box and it assigns the value to the box according to that number, which is called the mass measurement. In multifractal analysis, ImageJ software sets an arbitrary exponent called Q to several values symmetrically distributed around 0 (for example -3, -2, -1, 0, 1, 2, 3). Following that, each mass measurement is emphasized by being raised to Q, and corresponding fractal dimensions denoted D_{-3}, D_{-2}, D_{-1}, D_0, D_1, D_2 and D_3 are calculated. If the structure that is being analyzed has a multifractal nature, then $D_0>D_1>D_2$. The f(α) curve is commonly used for interpretation of multifractal analysis. This is a convex curve, and its aperture from 1 to -1, as well as the aperture slope can be used for overall assessment of the multifractal results that include for all values of Q (35).

6) Statistical analysis

T-test and one-way ANOVA with Tukey post-hoc test were performed by using the statistical program R. In order to measure the inter-rater variability, we calculated free-marginal kappa, a chance-adjusted measure of agreement for any number of cases, categories, or raters by using free on-line calculator (36).

RESULTS

1) Automatic segmentation of images

The application of the automatic segmentation method produced gray scale images that specifically showed the vascular network details to high order of branching generations without artifacts from laser treatment, hemorrhages, and exudates. In addition, the use of two types of filters produced two sets of images. The application of the coarse filter resulted in a set of binarized vascular network images with a low number of vessel branching generations: vessel branches from the first to approximately the fourth generation of branching. The application of the fine filter yielded a set of binarized images with a high number of vessel branching generations that also included vessels belonging to more than four generations of branching (Figure 3).

2) Box-counting dimension and lacunarity of DIARETDB1 images with a high number of branching generations

Box-counting analysis of images with a high number of branching generations showed that the complexity of vascular network measured by the box-counting dimension Db increases as the severity of DR increases. At the same time, lacunarity (or gappiness, or inhomogeneity) decreases with more severe stages of DR (Figure 4A and 4B).

3) Multifractal dimensions of DIARETDB1 images with a high number of branching generations

The multifractal analysis of images with a high number of branching generations yielded results with the same trends as the results of the box-counting analysis (Table 2): as the severity of DR increased, the complexity of the vascular network increased as well. In addition, this analysis confirmed the multifractal nature of microvascular network in the retina, because the rule in which $D_0 > D_1 > D_2$ was satisfied.

The analysis of f(α) spectra showed that the aperture length -1 to 1 is significantly shorter in the severe DR group, and the aperture slope has a more downward trend when compared to the moderate DR group (Figure 5).

4) Comparison of images with a high number and a low number of vessel branching generations: STARE and DIARETDB1 database

We show that fractal characterization results of the microvascular network morphology in DR depend on the number of vessel branching generations that analysis takes into account. For example, analysis of DIARETDB1 images showed that the progressive increase of complexity and progressive decrease in gappiness of the microvascular network were associated with the increased severity of DR only if the microvessels of higher order of branching were included in the analysis (Table 2, Figure 6). However, the box-counting analysis of corresponding images with low number of vessel branching generations failed to show significant difference in complexity among the groups. In addition, the lacunarity analysis of the same set of images with low number of vessel generations showed that gappiness in the severe DR was actually increased when compared to the moderate DR (mean lacunarity ± SD, 0.614 ± 0.086 for the normal looking vs. 0.5418 ± 0.0372 for the moderate vs. 0.6375 ± 0.0634 for the severe DR, p=0.031, data not shown).

The results of our previous report (27) support this observation. In that report we used raw retinal images from the STARE database. It is important to emphasize that the resolution of these images was significantly lower compared to the DIARETDB1 images. Therefore, the level of details and the number branching generations on corresponding manually segmented images was relatively low. In that report, the analysis of these manually segmented STARE images showed that microvascular network in PDR displays increased lacunarity and decreased fractal dimension when compared to the healthy retinas. To explore this further, in the study we present here we performed the same automatic segmentation of the STARE images and applied the same filters as for the DIARETDB1 images. Similar to manually segmented images, after automatic segmentation the lacunarity analysis of set of images with low number of vessel branching generations showed that PDR group displays increased lacunarity when compared to the healthy group. Also, the box-counting analysis of the set with a high number of branching generations showed the that complexity was higher in PDR, which was

consistent with the observation from analysis of DIARETDB1 images with the high number of branching generations (Table 3).

The multifractal analysis of images with low number of vessel branching generations did not demonstrate any significant changes in the microvascular complexity related to severity of DR (data not shown).

DISCUSSION

The analysis of DIARETDB1 images with a high number of branching generations showed that the increase in severity of DR is associated with increased complexity of microvascular network measured by box-counting dimension. At the same time, this is associated with decreased gappiness or inhomogeneity as measured by lacunarity. In addition, we show that severe stages of DR are characterized by smaller aperture length of the f(α) spectra, when compared to moderate DR.

Taken together our results demonstrate that microvascular geometry typical for severe stages of DR could be detected by a simple, inexpensive, non-invasive automated method based on high resolution fundus photography, automatic segmentation of microvasculature to the high number of branching generations and multifractal analysis of the retinal microvascular geometry. The application of non-mydriatic fundus camera in combination with telemedicine for DR screening has been already evaluated and implemented at the local level in Italy with the plan for developing a national screening program. It has been shown to be a very effective and affordable tool for the prevention of blindness caused by DM (37, 38). The application of the concept presented in our study at the primary care level could allow the inclusion of family physicians in the assessment of DR in all patients with DM at every visit regardless of the duration of the disease. This would alleviate assessment of diabetic patients and aid the timely diagnosis of advanced stages of DR. This could not only improve the prevention and slow down the progression of visual impairment, but it could be beneficial for the timely detection of the other diabetic microvascular complications (9). In addition, the population-level cohort study by Brownrigg et al. showed that the presence of microvascular complications in diabetes such as

peripheral neuropathy, nephropathy, and retinopathy significantly increased the risk of cardiovascular disease in patients with DM2 (11). The Brownrigg's study showed that the risk stratification for cardiovascular events significantly improved if the models accounted for cumulative microvascular disease burden. Moreover, the meta-analysis of 20 observational studies showed that DR in both DM1 and DM2 is associated with increased risk for all-cause mortality and cardiovascular events (fatal and non-fatal) (10). This risk doubled in individuals with severe DR, and the risk was present independently from the traditional cardiovascular risk factors. These data pointed out that evaluation of each patient with DM for the presence and severity of DR could improve their cardiovascular risk stratification. Furthermore, retinal and cerebral microvasculature share numerous anatomical and physiological features, so the presence of advanced stages of DR increases risk for the development of dementia (12). Therefore, the patients with changes typical for severe non-proliferative and proliferative DR should be referred promptly not only for the evaluation by an eye specialist, but also for further evaluation of CV risk by a cardiologist, and evaluation of risk for development of dementia by a neurologist.

In our study, moderate DR is characterized by the change of aperture length and slope of the f(α) spectra when compared to severe DR. However, the aperture length and slope of the f(α) spectra in the healthy looking group was not different from either group with DR. One of the reasons for this observation could be small sample size that was used in the study. According to the currently accepted standards of care, laser photocoagulation and intravitreal injections are the recommended methods for treatment of DR (39). These methods are invasive, associated with numerous side effects, and are reserved for severe stages of DR. Nevertheless, noninvasive therapeutic modalities like application of topical medications in early, preclinical stages of DR, in asymptomatic patients, are being developed (39). Therefore, detection of not only moderate DR, but also detection of very early, preclinical asymptomatic stages of DR are important especially from the standpoint of prevention of visual decline due to diabetes. The early preclinical stage of DR is characterized by retinal neurodegeneration with the loss of neural cells in retina, and the visible microvascular changes are

still not detectable on color fundus photographs at that time (39). However, recent studies using OCTA imaging confirmed that, when compared to retinas of healthy people, subtle microvascular changes such as the enlargement of the foveolar avascular zone and perifoveolar capillary loss are present even in the preclinical stage (40) resulting in subtle, but important alterations in the microvascular network complexity in the region of macula. We could not test this in our study not only because of the small sample size and insufficient quality of images, but also because the information associated with retinal images in DIARETDB1 and STARE databases did not specify if the images of healthy looking retinas come from the healthy people with no DM, or from the people with DM and no clinical signs of the disease.

We show that the results of fractal analysis are affected by the number of vessel branching generations included in the analysis. The studies that examine how microvascular complexity changes in DR report conflicting results and our results might at least partially explain these inconsistencies. For example, Leontidis et al. found that complexity of vascular network decreases in early stages of DR in patients with DM2 (16). However, others show that in advanced DR fractal dimension of microvascular network increases especially in severe proliferative stages (17). Moreover, in patients with DM1, it has been shown that the complexity of the microvasculature increases in early DR even in the absence of neovascularization (18). These inconstancies may be related to the fact that different stages of the DR and different types of diabetes were analyzed in these studies. In addition to this, our results point out that different methods of microvascular network segmentation represent an important cause of these disagreements. Generally, the level of microvascular network details that are extracted from the raw image varies widely depending on the automatic segmentation method used, quality of raw fundus images, and in the cases of manual segmentation, on the expert performing the segmentation (27, 41). Some automatic segmentation methods and some of the manually segmented images display retinal blood vessels of a larger caliber and just a few subsequent generations of branching, while others are more detailed and also include smaller vessels with more branching generations (41).

Automatic segmentation used in this study displays the ability to segment blood vessels without artifacts from hemorrhages, exudates, and laser photocoagulation. This allowed the fractal analysis results to represent changes in microvascular geometry, without being influenced by the other changes in the retina typically observed in DR, or by any technical artifacts. Moreover, this automatic method segmented images of the microvascular network to the high level of details. Nevertheless, the method was sensitive to large variations in light exposure when capturing the image and this study emphasizes the importance of calibration and standardization of conditions for capturing the retinal fundus images. High level of details in segmented images allowed us to use 2 filters to generate the set of images with a high, and the corresponding set of images with a low number of branching generations, and to characterize how microvascular geometry at different branching levels of vascular tree changes with the progression of DR. Marupally et al. used similar “two-pronged approach” for processing of retinal fundus images in DR, in which one set of filtering conditions was used for the semi-automated detection of bright hard exudates, and a different set for the detection of faint hard exudates (42). However, their approach did not focus on the analysis of microvascular network complexity.

There are number of limitations to this study. The study reports values for only a small number of color fundus images with or without signs of diabetic retinopathy, but without any additional associated information. Report recently published by Vujosevic et al. demonstrates that in the assessment of changes associated with DR, the type of DM is important (40). Therefore, additional large scale studies are necessary to account for relevant demographic information like race, age and gender, or any relevant medical history (duration and type of diabetes, type of therapy and compliance with it, presence of DM complications, smoking status) and laboratory findings (hemoglobin A1C, albuminuria, lipid profile). Information on the presence of other systemic diseases, as well as diseases specific to the eye that could also be associated with changes in microvascular network morphology was not available, and is out of the scope of this study, but should be addressed in the future as well.

PERSPECTIVES

Our results establish the fact that severe stages of non-proliferative and proliferative DR could be detected non-invasively by using a basic high resolution fundus photography and automatic segmentation of microvasculature to the high number of branching generations, followed by box-counting, lacunarity and multifractal analysis of retinal microvasculature.

This approach shows that the increase in the severity of DR is associated with increased complexity of the microvascular network as measured by fractal dimension, and decreased inhomogeneity of retinal microvascular network as measured by lacunarity.

Finally, we show that the results of fractal analysis are affected by the ability of a segmentation method to account for the smaller vessels with more branching generations.

TABLES

Table 1. Cumulative list of the data used in the study

DIARETDB1		STARE	
Image #	Diagnosis (DR stage)	Image#	Diagnosis
5	severe	077	Normal
8	severe	081	Normal
12	moderate	082	Normal
15	severe	085	PDR
17	severe	087	PDR
19	severe	162	Normal
20	severe	163	Normal
21	severe	179	PDR
30	healthy looking	204	PDR
33	healthy looking	232	PDR
34	healthy looking	235	Normal
43	moderate	236	Normal
50	healthy looking	239	Normal
52	moderate	240	Normal
54	moderate	255	Normal
56	moderate	342	PDR
58	moderate	343	PDR
66	severe	347	PDR
67	severe	351	PDR
72	healthy looking		

Table 2. Multifractal analysis - DIARETDB1 images with a high number of branching generations

	Mean ± SD for			
D (Q)	normal looking	moderate DR	severe DR	P-value
Q = 0, capacity dimension	1.7014^{a} ±0.0380	$1.7288^{a,b}$ ± 0.0139	1.7486^{b} ± 0.230	0.014
Q = 1, information dimension	1.6527^{a} ± 0.0366	$1.6723^{a,b}$ ± 0.0223	1.7063^{b} ± 0.0262	0.008
Q = 2, correlation dimension	1.6242^{a} ± 0.0356	$1.6417^{a,b}$ ± 0.0269	1.6810^{b} ± 0.0285	0.007

^{a,b} groups labeled with different letters are statistically different

Table 3. Summary of the box-counting and lacunarity analysis results on images from STARE database after automatic segmentation

Number of vessel branching generations	Type of analysis	Mean values ± SD		p-values
		Normal	PDR	
Low	Box-counting dimension	1.7556 ± 0.0063	1.7504 ± 0.0070	0.109
	Lacunarity	0.3228 ± 0.0186	0.3541 ± 0.0371	0.030
High	Box-counting dimension	1.7671 ± 0.0016	1.7703 ± 0.0022	0.002
	Lacunarity	0.2795 ± 0.0066	0.2745 ± 0.0097	0.204

FIGURE LEGENDS

Figure 1. Image processing work flow. Two-dimensional color retinal images of patients with diabetes mellitus from the publicly available DIARETDB1 and STARE databases were used in the study (14, 15, 25, 26). STEP 1: The images were segmented by the automatic method of blood vessel segmentation that originated from the RETINAL 2020 project. (28). STEP 2: The fine and the coarse filtering settings and thresholding were used on each image to generate one binarized image with the low, and the second image with the high number of vessel branching generations. STEP 3: vascular network morphology in different stages of diabetic retinopathy progression was compared by fractal analysis parametrization such as box/count dimension, lacunarity and multifractals in the set of images with low number of branching generations, as well as in the set with a high number of branching generations.

Figure 2. Estimation of the illumination settings for the raw color fundus images. A) The top panel shows an adequately exposed image, while the bottom panel shows the underexposed image. The corresponding mean histogram values from the GIMP image editor Value histogram function are shown as well. B) The graph shows the distribution of the mean histogram values (distribution of images by estimated light exposure values) for all 89 DIARETDB1 images. Twenty images belonging to the 4th quartile (mean exposure values from 105.7 to 159.25) were used in further analysis.

Figure 3. Results of the automatic segmentation. A) A raw image from the DIARETDB1 database (15, 16). White arrows pointing to the exudates, hemorrhages, and laser photocoagulation changes. B) Exudates, hemorrhages, and photocoagulation changes are not present on the corresponding segmented gray scale region of interest (ROI). C) Detail from the raw image, 4X enlarged. D) Detail from the gray scale segmented image, 4X enlarged. E) The ROI after the fine filter, thresholding and binarization were applied resulting in high number of vessel branching generations. F) The ROI after the coarse filter, thresholding, and binarization were applied resulting in low number of vessel branching generations.

Figure 4. Box-counting and lacunarity analysis of DIARETDB1 images with a high number of branching generations. A) Box-counting dimension Db, a measure of microvascular network complexity increases with severity of DR (mean box-counting dimension ± SD, 1.6397 ± 0.0308 for normal looking vs. 1.6622 ± 0.0159 for moderate DR vs. 1.6868 ± 0.0260 for severe DR, p=0.011), B) Lacunarity, a measure of gappiness decreases as the severity of DR retinopathy increases (mean lacunarity ± SD, 0.4881 ±0.0571 for normal looking vs. 0.4344 ±0.0506 for moderate DR vs. 0.3925 ± 0.0533 for severe DR, p=0.0175). Groups labeled with different letters are statistically different.

Figure 5. Multifractal analysis f(α) spectra – DIARETDB1 images with a high number of branching generations. A) f(α) spectra of images in: top - normal looking, middle - moderate DR,

bottom panel - severe DR. B) Aperture length from -1 to 1 in the severe DR group is shorter than in the moderate DR group (mean aperture length ± SD, 0.4620 ± 0.0367 for the normal looking vs. 0.4707 ± 0.0634 for the moderate vs. 0.4023 ± 0.045 for the severe DR, p=0.033). C) Aperture slope from -1 to 1 of the moderate DR group has a less downward trend compared to the severe DR group (mean aperture slope ± SD, -0.2803 ± 0.0199 for the normal looking vs. -0.2526 ± 0.0262 for the moderate DR vs. -0.280 ± 0.0093 for the severe DR, p=0.047). Groups labeled with different letters are statistically different.

Figure 6. Comparison of the images with a high and with a low number of vessel branching generations. Images with a low number of vessel branching generations are on the left side: A) normal looking, C) moderate DR, E) severe DR. Corresponding images with high number of vessel branching generations are on the right side: B) normal looking, D) moderate DR, F) severe DR. More severe DR associated with increased complexity and decreased in gappiness of retinal microvasculature can be observed only in images with a high number of vessel branching generations.

REFERENCES

1. *Global report on diabetes*. World Health Organization. http://www.who.int/diabetes/global-report/en/. Published 2018. Accessed October 7, 2018.

2. Cheng Y, Imperatore G, Geiss L et al. Secular Changes in the Age-Specific Prevalence of Diabetes Among U.S. Adults: 1988–2010. *Diabetes Care*. 2013;36(9):2690-2696. doi:10.2337/dc12-2074

3. *Life Expectancy*. Our World in Data. https://ourworldindata.org/life-expectancy. Published 2018. Accessed October 7, 2018.

4. Brandle M, Zhou H, Smith B et al. The Direct Medical Cost of Type 2 Diabetes. *Diabetes Care*. 2003;26(8):2300-2304. doi:10.2337/diacare.26.8.2300

5. *Priority eye diseases*. World Health Organization. http://www.who.int/blindness/causes/priority/en/. Published 2018. Accessed October 7, 2018.

6. 10. Microvascular Complications and Foot Care:Standards of Medical Care in Diabetes—2018. *Diabetes Care*. 2017;41(Supplement 1):S105-S118. doi:10.2337/dc18-s010

7. Spijkerman A, Dekker J, Nijpels G et al. Microvascular Complications at Time of Diagnosis of Type 2 Diabetes Are Similar Among Diabetic Patients Detected by Targeted Screening and Patients Newly Diagnosed in General Practice: The Hoorn Screening Study. *Diabetes Care*. 2003;26(9):2604-2608. doi:10.2337/diacare.26.9.2604

8. Gupta A, Gupta A, Singh T. Occurrence of complications in newly diagnosed type 2 diabetes patients: a hospital based study. *Journal of the Indian Medical Association*. 2013;111(4):245-7.

9. Cheung C, Thomas G, Tay W et al. Retinal Vascular Fractal Dimension and Its Relationship With Cardiovascular and Ocular Risk Factors. *Am J Ophthalmol*. 2012;154(4):663-674.e1. doi:10.1016/j.ajo.2012.04.016

10. Kramer C, Rodrigues T, Canani L, Gross J, Azevedo M. Diabetic Retinopathy Predicts All-Cause Mortality and Cardiovascular Events in Both Type 1 and 2 Diabetes: Meta-analysis of observational studies. *Diabetes Care*. 2011;34(5):1238-1244. doi:10.2337/dc11-0079

11. Brownrigg J, Hughes C, Burleigh D et al. Microvascular disease and risk of cardiovascular events among individuals with type 2 diabetes: a population-level cohort study. *The Lancet Diabetes & Endocrinology*. 2016;4(7):588-597. doi:10.1016/s2213-8587(16)30057-2

12. Exalto L, Biessels G, Karter A, Huang E, Quesenberry C, Whitmer R. Severe Diabetic Retinal Disease and Dementia Risk in Type 2 Diabetes. *Journal of Alzheimer's Disease*. 2014;42(s3):S109-S117. doi:10.3233/jad-132570

13. Romero P, Sagarra R, Ferrer J, Fernández-Ballart J, Baget M. The incorporation of family physicians in the assessment of diabetic retinopathy by non-mydriatic fundus camera. *Diabetes Res Clin Pract*. 2010;88(2):184-188. doi:10.1016/j.diabres.2010.02.001

14. Kauppi T, Kalesnykiene V, Kamarainen J et al. the DIARETDB1 diabetic retinopathy database and evaluation protocol. *Procedings of the British Machine Vision Conference 2007*. 2007. doi:10.5244/c.21.15

15. DIARETDB1 - STANDARD DIABETIC RETINOPATHY DATABASE. It.lut.fi. http://www.it.lut.fi/project/imageret/diaretdb1/. Published 2018. Accessed October 7, 2018.

16. Leontidis G, Al-Diri B, Wigdahl J, Hunter A. Evaluation of geometric features as biomarkers of diabetic retinopathy for characterizing the retinal vascular changes during the progression of diabetes. *2015 37th Annual International Conference of the IEEE Engineering in Medicine and Biology Society (EMBC)*. 2015. doi:10.1109/embc.2015.7319577

17. Daxer A. Characterisation of the neovascularisation process in diabetic retinopathy by means of fractal geometry: diagnostic implications. *Graefe's Archive for Clinical and Experimental Ophthalmology*. 1993;231(12):681-686. doi:10.1007/bf00919281

18. Cheung N, Donaghue K, Liew G et al. Quantitative Assessment of Early Diabetic Retinopathy Using Fractal Analysis. *Diabetes Care*. 2008;32(1):106-110. doi:10.2337/dc08-1233

19. Hwang T, Jia Y, Gao S et al. OPTICAL COHERENCE TOMOGRAPHY ANGIOGRAPHY FEATURES OF DIABETIC RETINOPATHY. *Retina*. 2015;35(11):2371-2376. doi:10.1097/iae.0000000000000716

20. 6. 2.5. *Histogram dialog*. Docs.gimp.org. https://docs.gimp.org/2.8/en/gimp-histogram-dialog.html. Published 2018. Accessed October 7, 2018.

21. Early Treatment Diabetic Retinopathy Study Design and Baseline Patient Characteristics. *Ophthalmology*. 1991;98(5):741-756. doi:10.1016/s0161-6420(13)38009-9

22. Online Self-Directed Diabetic Retinopathy Grading Course. Drgrading.iehu.unimelb.edu.au. http://drgrading.iehu.unimelb.edu.au/cera/index.asp. Published 2018. Accessed December 5, 2018.

23. Krause J, Gulshan V, Rahimy E et al. Grader Variability and the Importance of Reference Standards for Evaluating Machine Learning Models for Diabetic Retinopathy. *Ophthalmology*. 2018;125(8):1264-1272. doi:10.1016/j.ophtha.2018.01.034

24. Thapa R, Bajimaya S, Bouman R et al. Intra- and inter-rater agreement between an ophthalmologist and mid-level ophthalmic personnel to diagnose retinal diseases based on fundus photographs at a primary eye center in Nepal: the Bhaktapur Retina Study. *BMC Ophthalmol*. 2016;16(1). doi:10.1186/s12886-016-0295-0

25. *The STARE Project*. Cecas.clemson.edu. http://cecas.clemson.edu/~ahoover/stare/. Published 2018. Accessed October 7, 2018.

26. Hoover A, Kouznetsova V, Goldbaum M. Locating blood vessels in retinal images by piecewise threshold probing of a matched filter response. *IEEE Trans Med Imaging*. 2000;19(3):203-210. doi:10.1109/42.845178

27. Popovic N, Radunovic M, Badnjar J, Popovic T. Fractal dimension and lacunarity analysis of retinal microvascular morphology in hypertension and diabetes. *Microvasc Res*. 2018;118:36-43. doi:10.1016/j.mvr.2018.02.006

28. Retinal imaging prevention and early detection of chronic diseases | Projects | H2020 | CORDIS | European Commission. CORDIS | European Commission. https://cordis.europa.eu/project/rcn/216353_en.html. Published 2018. Accessed October 7, 2018.

29. Maninis K, Pont-Tuset J, Arbeláez P, Van Gool L. Deep Retinal Image Understanding. *Medical Image Computing and Computer-Assisted Intervention – MICCAI 2016*. 2016:140-148.

doi:10.1007/978-3-319-46723-8_17

30. Staal J, Abramoff M, Niemeijer M, Viergever M, van Ginneken B. Ridge-Based Vessel Segmentation in Color Images of the Retina. *IEEE Trans Med Imaging*. 2004;23(4):501-509. doi:10.1109/tmi.2004.825627

31. Owen C, Rudnicka A, Mullen R et al. Measuring Retinal Vessel Tortuosity in 10-Year-Old Children: Validation of the Computer-Assisted Image Analysis of the Retina (CAIAR) Program. *Investigative Opthalmology & Visual Science*. 2009;50(5):2004. doi:10.1167/iovs.08-3018

32. Odstrcilik J, Kolar R, Kubena T et al. Retinal vessel segmentation by improved matched filtering: evaluation on a new high-resolution fundus image database. *IET Image Process*. 2013;7(4):373-383. doi:10.1049/iet-ipr.2012.0455

33. Campbell J, Zhang M, Hwang T et al. Detailed Vascular Anatomy of the Human Retina by Projection-Resolved Optical Coherence Tomography Angiography. *Sci Rep*. 2017;7(1). doi:10.1038/srep42201

34. Rasband W. ImageJ. Rsb.info.nih.gov. http://rsb.info.nih.gov/ij/. Published 2018. Accessed October 7, 2018.

35. Karperien A, Jelinek H. Box-Counting Fractal Analysis: A Primer for the Clinician. *Springer Series in Computational Neuroscience*. 2016:13-43. doi:10.1007/978-1-4939-3995-4_2

36. Online Kappa Calculator. Justusrandolph.net. http://justusrandolph.net/kappa/. Published 2018. Accessed December 5, 2018.

37. Vujosevic S, Midena E. Diabetic Retinopathy in Italy: Epidemiology Data and Telemedicine Screening Programs. *J Diabetes Res*. 2016;2016:1-6. doi:10.1155/2016/3627465

38. Scarpa G, Urban F, Vujosevic S et al. The Nonmydriatic Fundus Camera in Diabetic Retinopathy Screening: A Cost-Effective Study with Evaluation for Future Large-Scale Application. *J Ophthalmol*. 2016;2016:1-7. doi:10.1155/2016/4625096

39. Simó R, Hernández C. Neurodegeneration in the diabetic eye: new insights and therapeutic perspectives. *Trends in Endocrinology & Metabolism*. 2014;25(1):23-33.

doi:10.1016/j.tem.2013.09.005

40. Vujosevic S, Muraca A, Alkabes M et al. EARLY MICROVASCULAR AND NEURAL CHANGES IN PATIENTS WITH TYPE 1 AND TYPE 2 DIABETES MELLITUS WITHOUT CLINICAL SIGNS OF DIABETIC RETINOPATHY. *Retina*. 2017:1. doi:10.1097/iae.0000000000001990

41. Badnjar J, Popovic N, Radunovic M, Popovic T. Retinal Blood Vessel Segmentation: Dijkstra Forest and Multi-Scale Line Detection Methods. 22Nd International Scientific/Professional Information Technology Conference, 2017: pp. 110-113. http://www.it.ac.me/zbornici/Zbornik%20IT17.pdf. Published 2018. Accessed October 7, 2018.

42. Marupally A, Vupparaboina K, Peguda H, Richhariya A, Jana S, Chhablani J. Semi-automated quantification of hard exudates in colour fundus photographs diagnosed with diabetic retinopathy. *BMC Ophthalmol*. 2017;17(1). doi:10.1186/s12886-017-0563-7

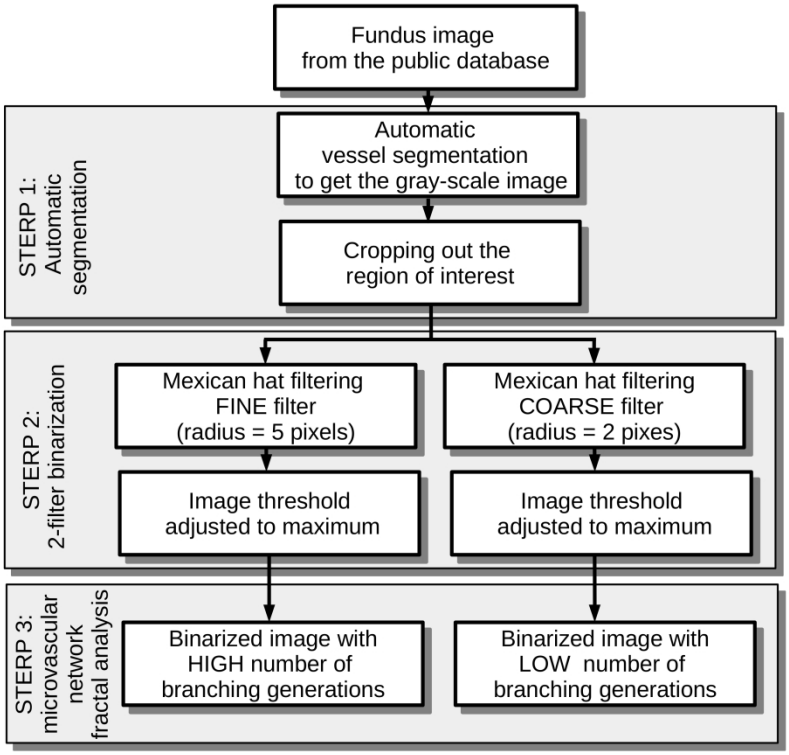

Figure 1. Image processing work flow. Two-dimensional color retinal images of patients with diabetes mellitus from the publicly available DIARETDB1 and STARE databases were used in the study (14, 15, 25, 26). STEP 1: The images were segmented by the automatic method of blood vessel segmentation that originated from the RETINAL 2020 project. (28). STEP 2: The fine and the coarse filtering settings and thresholding were used on each image to generate one binarized image with the low, and the second image with the high number of vessel branching generations. STEP 3: vascular network morphology in different stages of diabetic retinopathy progression was compared by fractal analysis parametrization such as box/count dimension, lacunarity and multifractals in the set of images with low number of branching generations, as well as in the set with a high number of branching generations.

280x209mm (299 x 299 DPI)

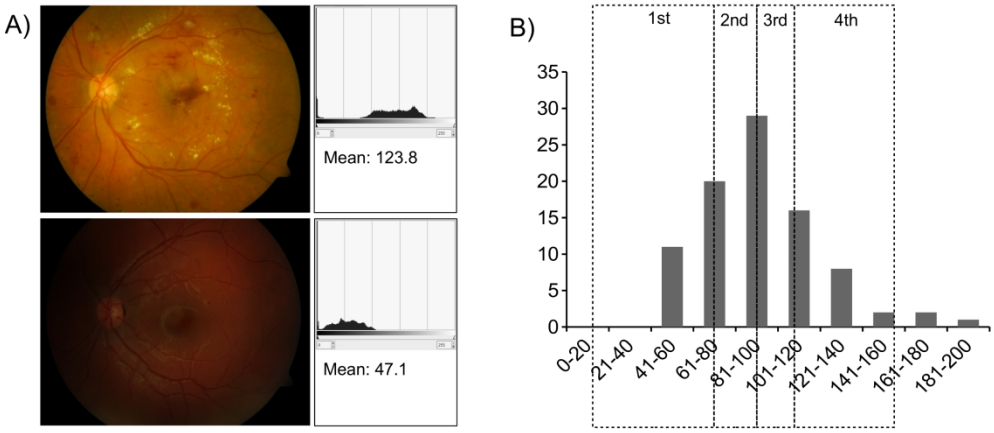

Figure 2. Estimation of the illumination settings for the raw color fundus images. A) The top panel shows an adequately exposed image, while the bottom panel shows the underexposed image. The corresponding mean histogram values from the GIMP image editor Value histogram function are shown as well. B) The graph shows the distribution of the mean histogram values (distribution of images by estimated light exposure values) for all 89 DIARETDB1 images. Twenty images belonging to the 4th quartile (mean exposure values from 105.7 to 159.25) were used in further analysis.

247x108mm (300 x 300 DPI)

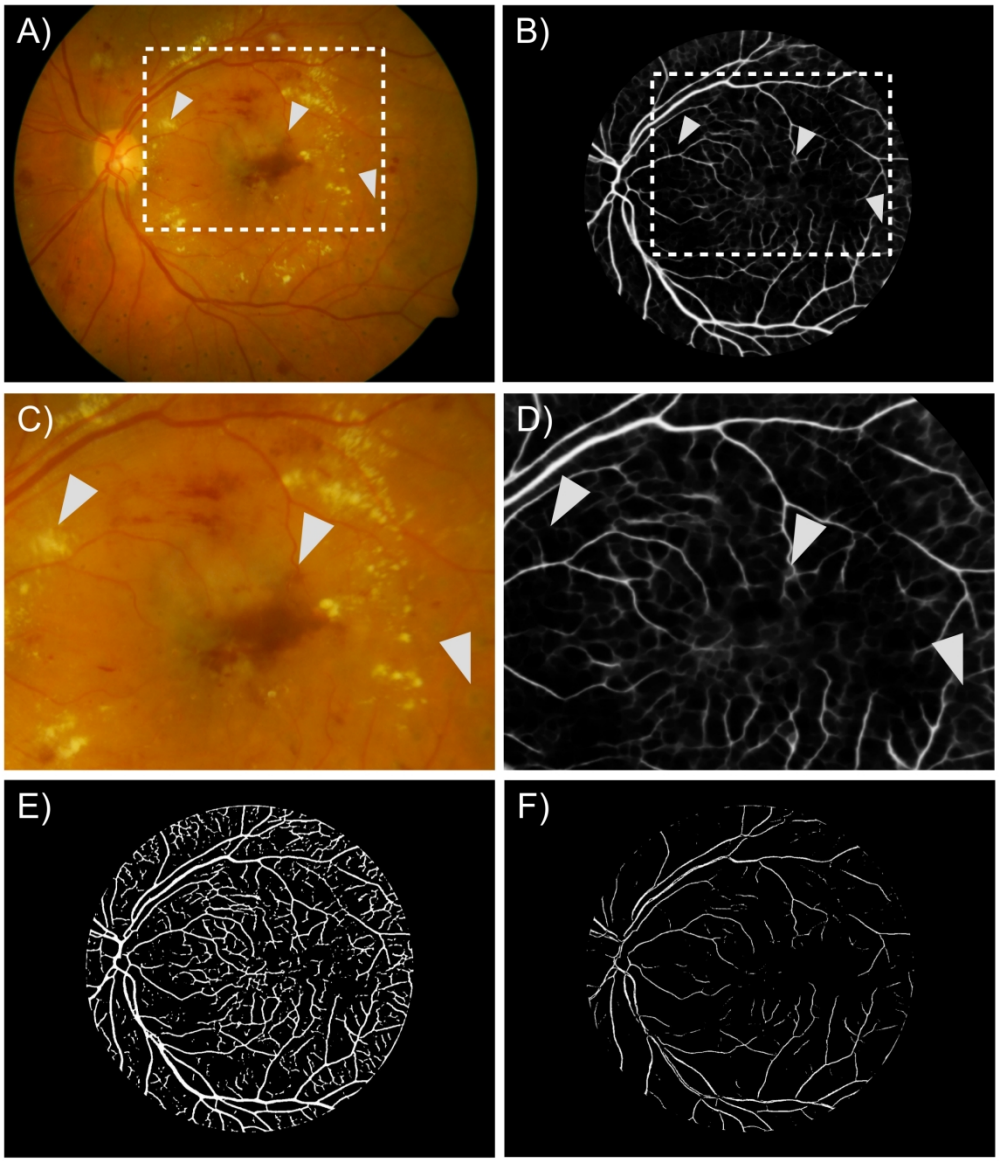

Figure 3. Results of the automatic segmentation. A) A raw image from the DIARETDB1 database (15, 16). White arrows pointing to the exudates, hemorrhages, and laser photocoagulation changes. B) Exudates, hemorrhages, and photocoagulation changes are not present on the corresponding segmented gray scale region of interest (ROI). C) Detail from the raw image, 4X enlarged. D) Detail from the gray scale segmented image, 4X enlarged. E) The ROI after the fine filter, thresholding and binarization were applied resulting in high number of vessel branching generations. F) The ROI after the coarse filter, thresholding, and binarization were applied resulting in low number of vessel branching generations.

201x234mm (300 x 300 DPI)

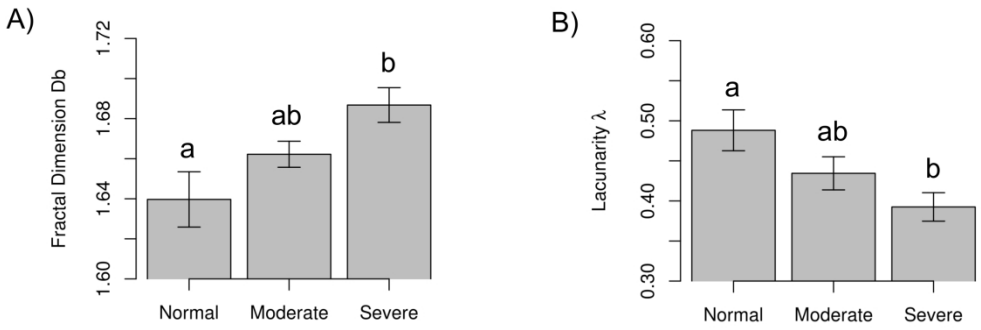

Figure 4. Box-counting and lacunarity analysis of DIARETDB1 images with a high number of branching generations. A) Box-counting dimension Db, a measure of microvascular network complexity increases with severity of DR (mean box-counting dimension ± SD, 1.6397 ± 0.0308 for normal looking vs. 1.6622 ± 0.0159 for moderate DR vs. 1.6868 ± 0.0260 for severe DR, p=0.011), B) Lacunarity, a measure of gappiness decreases as the severity of DR retinopathy increases (mean lacunarity ± SD, 0.4881 ±0.0571 for normal looking vs. 0.4344 ±0.0506 for moderate DR vs. 0.3925 ± 0.0533 for severe DR, p=0.0175). Groups labeled with different letters are statistically different.

228x79mm (300 x 300 DPI)

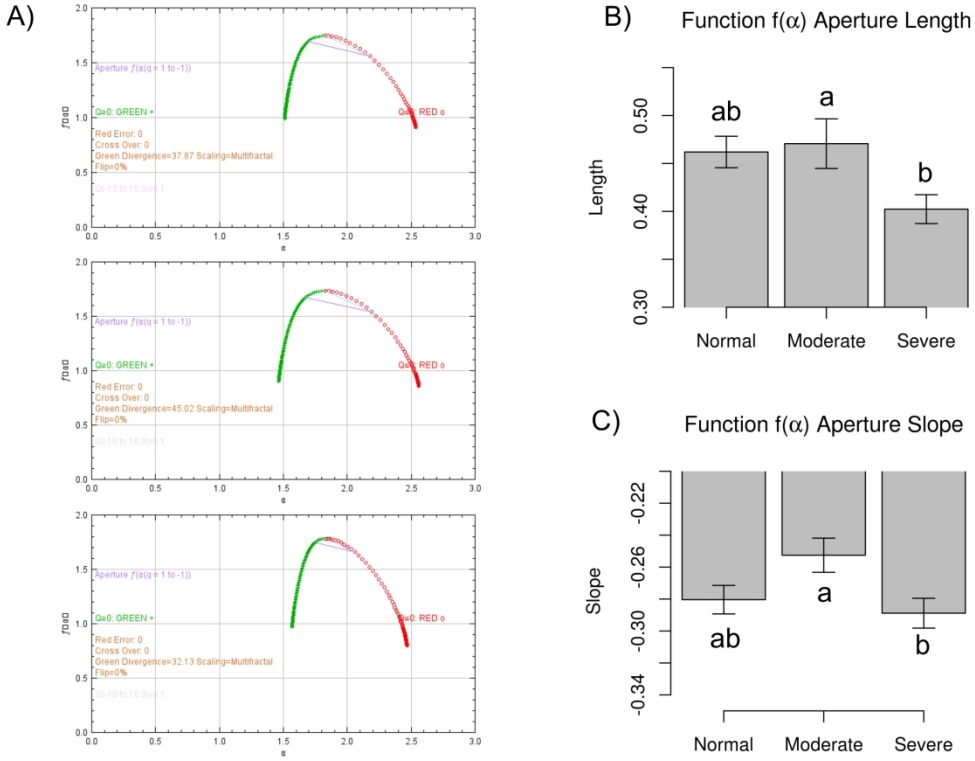

Figure 5. Multifractal analysis f(α) spectra – DIARETDB1 images with a high number of branching generations. A) f(α) spectra of images in: top - normal looking, middle - moderate DR, bottom panel - severe DR. B) Aperture length from -1 to 1 in the severe DR group is shorter than in the moderate DR group (mean aperture length ± SD, 0.4620 ± 0.0367 for the normal looking vs. 0.4707 ± 0.0634 for the moderate vs. 0.4023 ± 0.045 for the severe DR, p=0.033). C) Aperture slope from -1 to 1 of the moderate DR group has a less downward trend compared to the severe DR group (mean aperture slope ± SD, -0.2803 ± 0.0199 for the normal looking vs. -0.2526 ± 0.0262 for the moderate DR vs. -0.280 ± 0.0093 for the severe DR, p=0.047). Groups labeled with different letters are statistically different.

229x176mm (300 x 300 DPI)

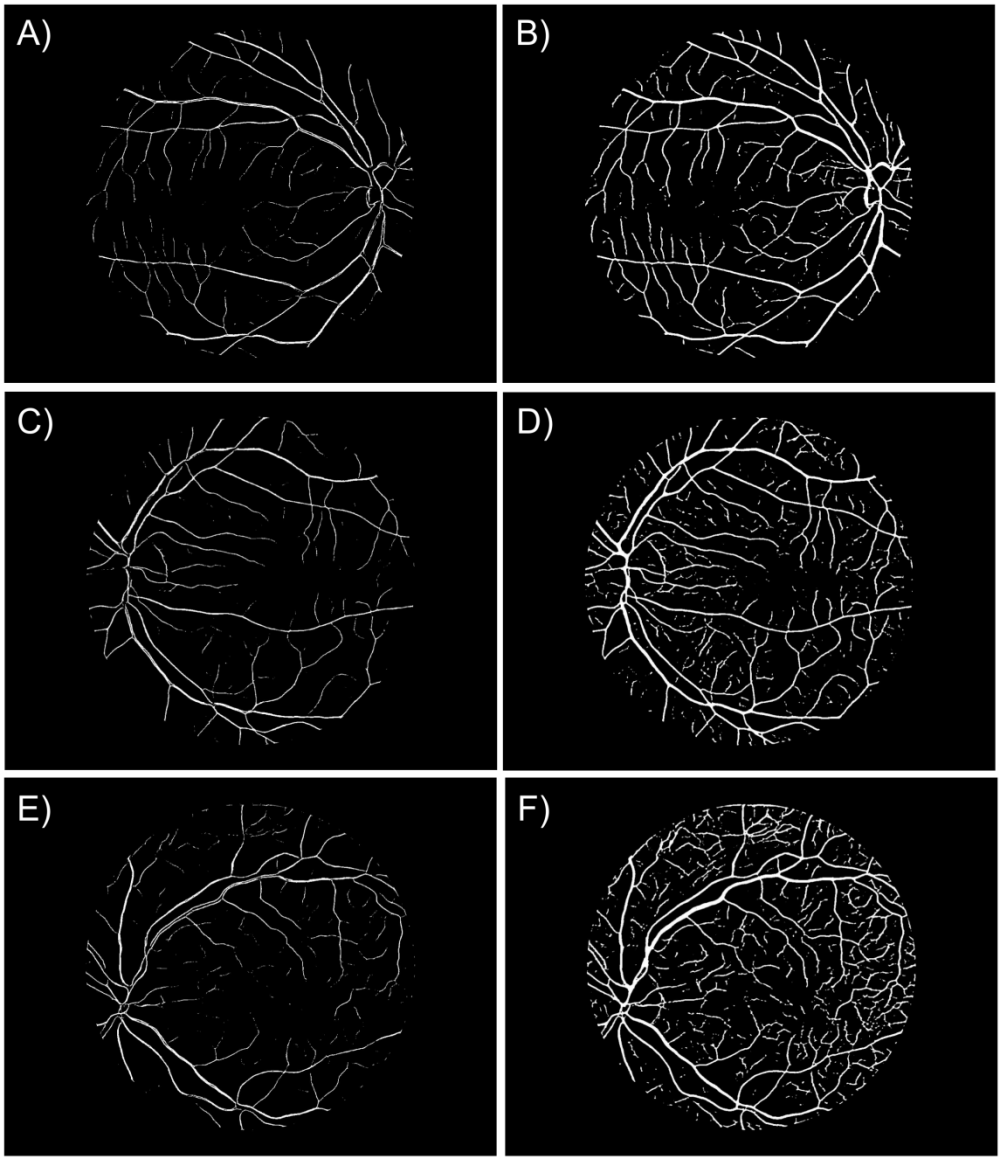

Figure 6. Comparison of the images with a high and with a low number of vessel branching generations. Images with a low number of vessel branching generations are on the left side: A) normal looking, C) moderate DR, E) severe DR. Corresponding images with high number of vessel branching generations are on the right side: B) normal looking, D) moderate DR, F) severe DR. More severe DR associated with increased complexity and decreased in gappiness of retinal microvasculature can be observed only in images with a high number of vessel branching generations.

201x233mm (300 x 300 DPI)